FISEVIER

Contents lists available at ScienceDirect

Journal of Power Sources

journal homepage: www.elsevier.com/locate/jpowsour



Short communication

A pseudo-solid-state cell for multiplatform *in situ* and *operando* characterization of Li-ion electrodes



Lin Feng^{a,*}, Zhijie Chen^a, Ruqi Chen^b, Shen J. Dillon^a

- ^a University of Illinois at Urbana-Champaign, Urbana, IL 61801, USA
- b Center of Experimental Teaching for Common Basic Courses, South Agricultural University, Guangzhou, 510642, China

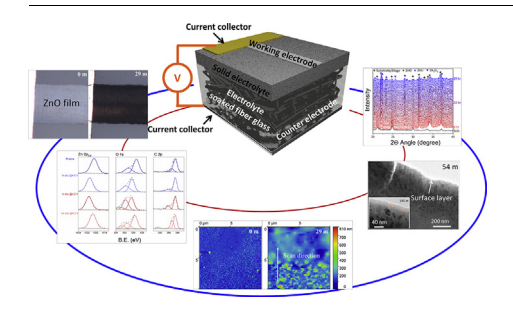
HIGHLIGHTS

- A novel and simple pseudo-solid-state Li ion battery platform has been designed.
- In situ TEM, AFM, SEM, XPS, and optical imaging are obtained from a ZnO anode
- New insights gained into the structural and chemical changes in ZnO during cycling.
- Changes in electrical properties are related to the microstructure evolution

ARTICLE INFO

Keywords: Li-ion battery In situ characterization Operando characterization Solid state battery

GRAPHICAL ABSTRACT



ABSTRACT

In the last decade, reacting Li ion electrodes *in situ* using vacuum based methods such as transmission electron microscopy (TEM) has become prevalent for assessing their reaction pathways. However, the vast majority of these studies do not perform electrochemical reactions at potentials relevant to batteries and/or characterize electrolytic reactions. Here we demonstrate a simple and flexible approach combining the benefits of solid and liquid electrolytes to enable diverse *in situ* characterization methods, including optical imaging, electrical measurements, X-ray photoelectron spectroscopy, X-ray diffraction, atomic force microscopy, and transmission electron microscopy. This work demonstrates these methods applied to the novel cell during electrolytic lithiation of the conversion anode ZnO at electrochemically relevant potentials.

Due to their sensitivity to environmental exposure and the importance of sample history in affecting reaction pathways, structural and analytical characterization of Li ion electrodes should ideally be performed *in situ* or *operando*. This fact has long been understood with *operando* X-ray diffraction being employed to study Li primary batteries as early as the 1970's [1]. However, rapid growth in the development and application of advanced *in situ* Li ion battery characterization techniques has primarily occurred in the last decade or so [2,3]. A variety of X-ray, optical, electron, and neutron based scattering, absorption, and spectroscopy approaches, as well as scan probe and

magnetic techniques, have been applied to *in situ* and *operando* Li ion characterization [4–7]. The topic has been the subject of several recent review articles that thoroughly discuss the state-of-the-art [3,8–10]. Techniques whose stimuli and resultant signal have long mean free paths can be applied relatively simply to electrochemical cells that are only slightly modified from standard laboratory or commercial formats. This explains why *in situ* X-ray diffraction was already being employed prior to the advent of commercial Li ion cells [1]. However, many techniques based on stimuli or signals with short mean free paths, such as low energy electrons, require the development of specialized

E-mail address: linfeng3@illinois.edu (L. Feng).

^{*} Corresponding author.

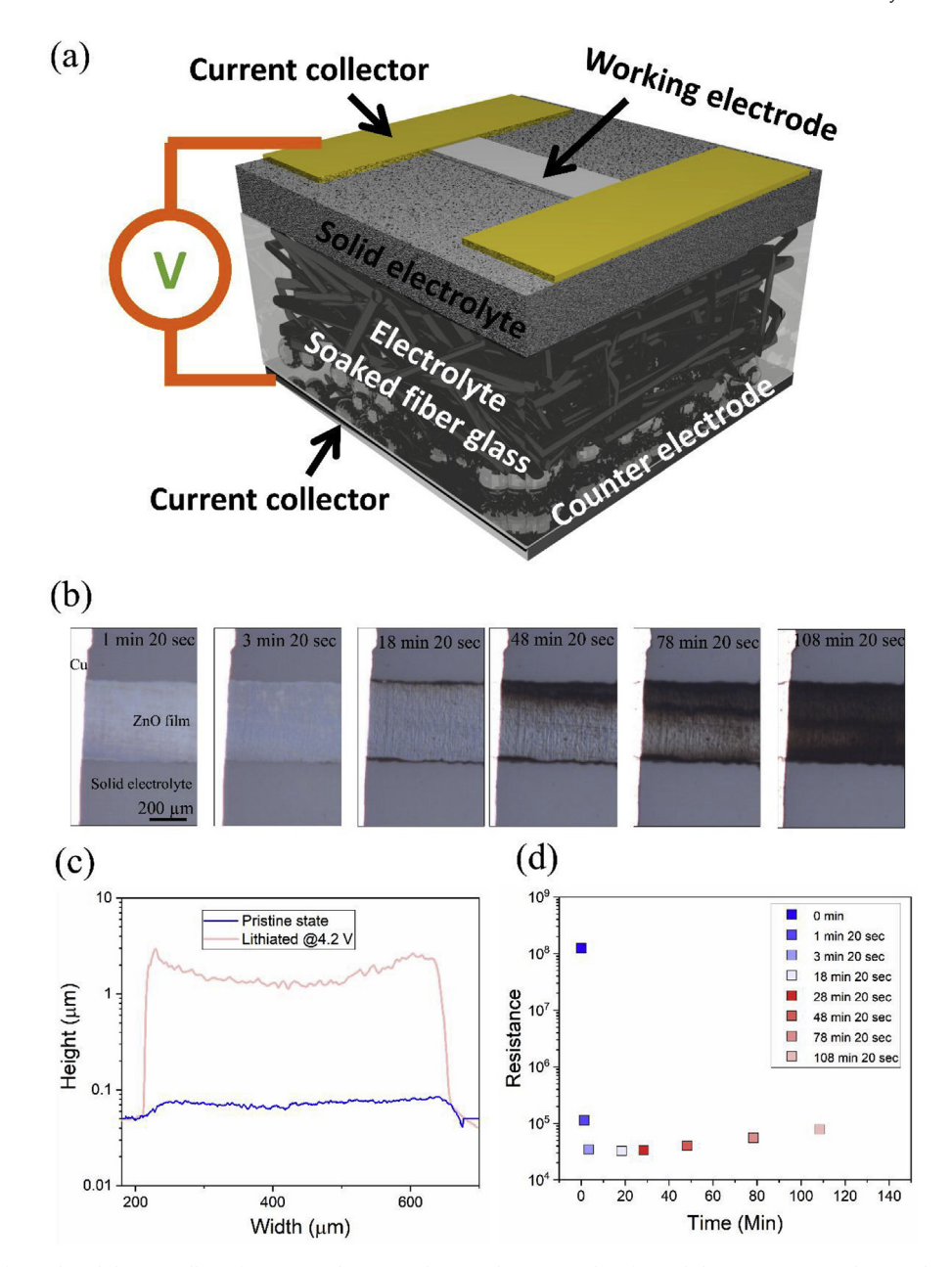


Fig. 1. (A) Schematic of pseudo-solid-state cell configuration; (b) *Operando* optical micrographs of ZnO lithiation at 4.2 V, along with (c) profilometry measured before and after the reaction, and (d) electrical conductivity measured intermittently.

electrochemical cells. For these reasons, in situ electron source and signal based approaches have primarily been developed in the past decade [2,11-16]. Unfortunately, many so-called "open cells" (i.e. reacting in vacuum) popular for electron-based characterization rely on electrochemically problematic cell designs. For example, > 100 in situ transmission electron microscopy (TEM) studies of Li induced reactions in vacuum have been reported in recent years [3], but most utilize galvanic reactions, often just direct chemical reactions with Li metal, and only a few demonstrate reactions at electrochemical potentials consistent with standard reactions or electrolytic reactions. Such studies often utilize overpotentials on the order of 3 V-5 V (e.g. -3 V to -5 Vversus Li metal or versus a cathode such as LiCoO2) to drive the reaction; see the following review for several examples [2]. These potentials are not electrochemically meaningful to Li ion batteries. This fact is important because the overpotential can affect the reaction pathway of the system. When measurements are made at poorly defined overpotentials it is unclear how the results relate to electrochemical batteries.

Solving scientific and engineering problems typically requires data from multiple sources and techniques. However, specialized electrochemical cells developed for one apparatus are often not amenable to use in different instrumentation. Experiments should be performed under similar electrochemical conditions for direct comparison, since reaction pathways can be sensitive to overpotential. Solid-state batteries are an ideal solution, since they can be cycled in vacuum, atmosphere, or submerged in liquids, they function well electrochemically, and can be characterized in almost any structural or analytical characterization equipment [17]. Certain solid electrolytes are less sensitive to X-ray and electron irradiation than liquid electrolyte. Reactions between liquid electrolyte and electrons or X-rays severely limited our prior in situ X-ray photoelectron spectroscopy (XPS) and TEM experiments [11,18,19]. Unfortunately, solid-state batteries are notoriously difficult and time consuming to fabricate, particularly outside of dedicated laboratories [20]. Here we seek to develop and demonstrate a flexible in situ Li ion cell amenable to multiplatform characterization that can be constructed simply using commercially

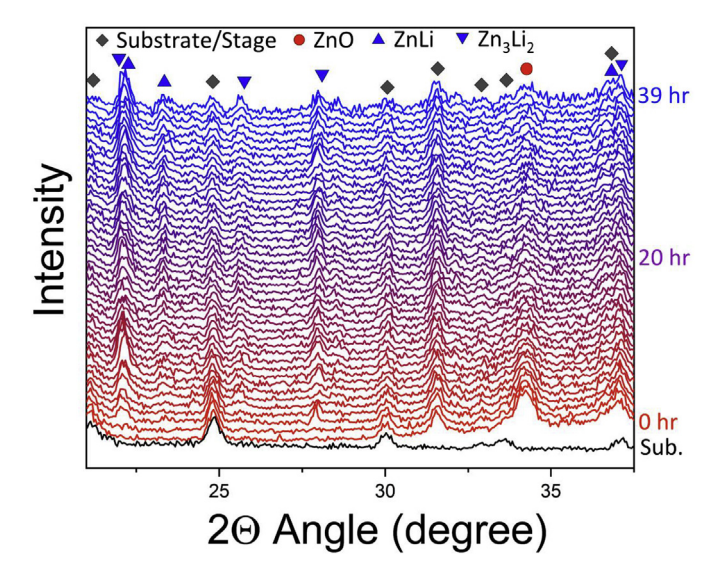


Fig. 2. Operando XRD measured during lithiation at 4.2 V at regular intervals over 39 h plotted along with the background peaks measured from the substrate.

available electrolyte and Li containing counter electrodes. To achieve this goal, we develop a pseudo-solid-state cell that combines both liquid and solid electrolytes, where the solid electrolyte serves as a convenient substrate for in situ characterization of the working electrode. The concept is to utilize commercially available Li₂Al₂SiTiP₂O₁₃ glassceramic electrolyte as a substrate for the working electrode, and contact the counter electrode through an intermediate liquid electrolyte. These solid electrolytes have been used to construct electrochemical cells that isolate two liquid electrolytes [21]. However, alone they cannot serve as the basis for solid-state batteries. Their lack of function in solid-state batteries likely results from charge transfer to the electrolyte, which can lead to a high impedance electrode-electrolyte interphase [22]. While this phenomenon has not been studied in this material in detail, similar behaviour has been observed in other systems [22,23]. Charge transfer to the electrolyte can be suppressed by coating a thin layer of insulator, such as $\approx 1 \text{ nm}$ of Al_2O_3 [24], which is demonstrated herein. This simple approach based on commercially available cell constituents makes it easy to fabricate and implement in any system where twoelectrode contacts can be made.

Our pseudo-solid-state electrochemical cell serves as a platform for performing various in situ characterization techniques such as, optical microscopy, electrical measurements, atomic force microscopy (AFM), X-ray diffraction (XRD), TEM and XPS. We utilize ZnO thin films as model electrodes to validate the approach. ZnO undergoes significant crystallographic, structural, chemical, and bonding changes during lithiation making it well suited to characterization by diverse methods. ZnO is a potential anode material that undergoes a conversion reaction with Li to form Li₂O + Zn followed by Li intermetallic formation with Zn [25]. ZnO has a high theoretical capacity of 988 mAh g⁻¹ [26]. However, it is unlikely to find commercial application due to large hysteresis loss and its high anode potential. There is some thought that understanding conversion reactions and improving their function could lead to improvements in high energy density transition metal fluorides that function as conversion cathodes; e. g ZnF₂ [27]. Debate remains as to the relative importance of electronic conduction, diffusional transport, and particle nucleation in contributing to the large overpotential that limits their application. For example, it might be expected that conversion reactions lead to metal nanoparticle percolation and good electronic conductivity subsequent to lithiation. However, direct measurements are limited and a general understanding of how physical properties and surface chemistry evolve during cycling is largely absent from the literature. Here ZnO is utilized as a simple model thin film that can be easily grown with reproducible properties and oxidation state in order to validate our approach. However, the results do provide new insights into how this conversion electrode evolves during lithiation. This work will explore how the electrical properties, microstructure, and chemistry evolve during the conversion reaction in ZnO.

The surfaces of $1 \text{ mm} \times 5 \text{ mm} \times 5 \text{ mm}$ Li₂Al₂SiTiP₂O₁₃ solid electrolytes were initially prepared by atomic layer deposition growth of ≈1 nm of Al₂O₃. The material was grown at 80 °C, using trimethlaluminum (TMA) and H₂O precursor gases deposited over 20 cycles. Approximately, 30-40 nm of ZnO was sputtered onto this substrate using DC magnetron sputtering in Ar at room temperature. 100 nm Cu current collector layers were e-beam deposited onto ZnO at the sample periphery. Whatman fiber glass soaked with 10 wt% bis (trifluoromethane) sulfonimide lithium salt in 1-methyl-1-propylpyrrolidinium bis (trifluoromethanesulfonyl) imide) ionically connected the solid electrolyte and the counter electrodes. The counter electrodes were contacted to conductive stainless steel substrates. Electrically isolated Cu clips were utilized to contact the working electrodes. Two such Cu clips were employed for two probe electrical conductivity measurements made across the ZnO strip. During cycling cell is not sealed from the surrounding vacuum or atmospheric environment in any way. Schematics of the electrochemical cells and images of the test platforms are shown in Fig. 1 as well as Supplementary Fig. S1 and Fig. S2, respectively. In situ electrochemical cycling of the cell was performed using a digital potentiostat. Details related to each specific characterization method are provided in the Supplementary data. Cyclic voltammetry (CV) performed against Li metal, used as a pseudoreference for comparison to the literature, is shown in Supplementary Fig. S3. The CV curves versus Li match literature reports for ZnO nanoparticles reasonably well [28,29]. All other experiments performed herein utilize LiCoO2 counter electrodes, which form initially electrolytic cells.

Lithiation of a ≈ 40 nm ZnO film is imaged clearly by optical microscopy. Fig. 1 shows a time-lapse sequence associated with charging LiCoO₂ at 4.2 V versus ZnO; also see Video S1. Chronoamperometry associated with in situ experiment is shown in Supplementary Fig. S4. The initially transparent, but reflective, film progressively becomes darker and eventually almost completely black as Li inserts. The reaction appears to occur in at least two stages. It initially propagates along thin lines separated by regions of unreacted material. In the latter stage, a dark reaction front propagates from the edge of the film towards the centre. Profilometry (see Fig. 1(c)) was performed before and after lithiating this sample for 108 min. The sample height expands to ≈1600 nm on average, while almost no lateral or longitudinal expansion occurs due to substrate clamping. The 341% volume expansion measured by profilometry slightly exceeds the theoretical value of 315% [26], but is consistent with an approximately complete reaction. Electrical resistance was measured intermittently across this electrode; Fig. 1(d). In the first 1.3 min the resistance decreases by 3 orders of magnitude. This correlates with the appearance of brownish streaks of reacted material observed optically. The streaks percolate across the entire electrode and this reacted material is believed to carry most of the current accounting for the reduced electrical resistance. As the intermediate unreacted regions continue to react the resistance gradually decreases by a factor of 3, and after ≈ 3.3 min begins increasing again as a dark reaction front propagates across the sample. The resistance does not reduce to values that would be associated with metallic conduction.

Operando XRD was performed on 500 nm thick ZnO films over a period of 39 h, as shown in Fig. 2. Thicker films were used to improve signal-to-noise, but require longer reaction times to account for the increased diffusion distance. The (002) ZnO peak at 34.3° overlaps with a substrate peak at 33.8°, but throughout the reaction it clearly reduces in intensity, relative to the other substrate peaks. The appearance or new peaks at 22.1°, 23.4°, 25.7°, and 28.0 occurs during charging. Our results are similar to those in Ref. [30], which tracked lithiation of Zn

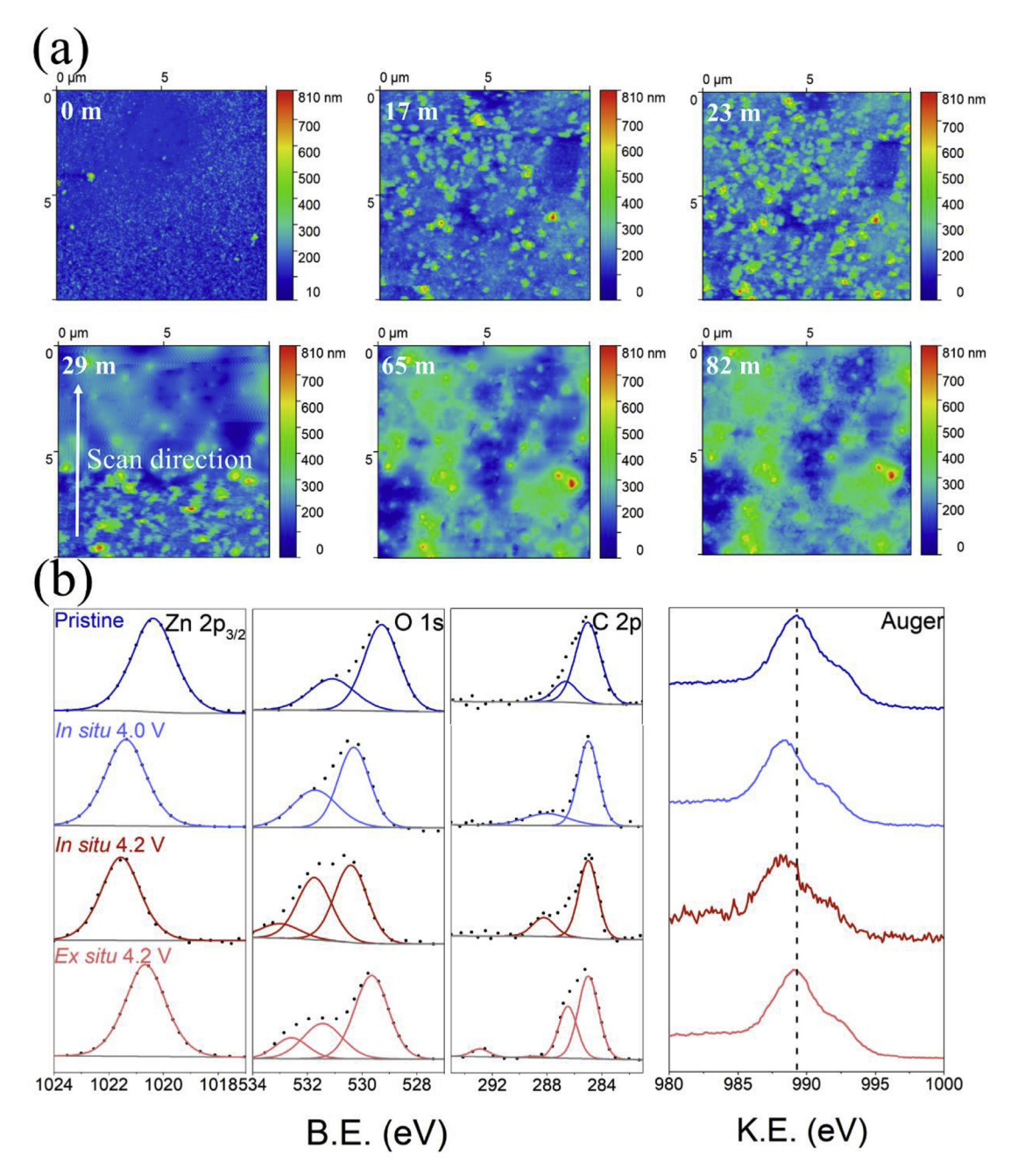


Fig. 3. (A) Operando AFM measured during lithiation at 4.2 V as well (b) as in situ and ex situ XPS measured at 4.0 and 4.2 V.

and observed ${\rm Li_2Zn_3}$ and LiZn phases. The multiple intermetallic phases result from sequential two phase reactions. These particles account for the optically black appearance of the reacted films in Fig. 1. These data both demonstrate the occurrence of the anticipated conversion reaction and the function of the cell. However, we note that the reaction may not have completed on the timescale of the experiment due to the thickness of the film, which is suggested by the presence of partially lithiated Zn. Since the reaction is performed in air, some surface oxidation may occur, but the observation of metallic phases and the optical properties suggest the material in the bulk ZnO is reduced.

Fig. 3 and Video S2 show time-lapse AFM topographic images associated with *operando* lithiation of a 40 nm ZnO film; see Supplementary Fig. S5 for associated phase images. During the first 23 min isolated protrusions develop on the surface. A reaction front rapidly moves through the field of view at ≈ 29 min as indicated by the discontinuous change in morphology. At longer times, the surface

morphology does not change appreciably. To understand the chemistry of this reaction layer, 40 nm thick samples were lithiated in situ in the XPS for 1 h at 4.0 V and 4.2 V versus LiCoO2. During prior in situ XPS experiments utilizing cells based on ionic liquid it was not possible to observe the same region of the sample multiple times due to the interaction of the X-rays with the liquid electrolyte [18,19,31,32]. However, the pseudo-solid state cell prevents the X-rays from interacting with the liquid electrolyte and its electrochemical function is not affected by the X-rays. The Zn $2p_{3/2}$, O 1s, C 1s, and Auger peaks are plotted in Fig. 3. The pristine Zn Auger and $2p_{3/2}$ peaks both correspond to ZnO. The Zn Auger peak is anticipated to shift 4 eV higher in kinetic energy during reduction to Zn metal. However, the Zn peak shifts ≈1 eV to lower kinetic energy, 988.2 eV, during lithiation at 4.0 V and 4.2 V versus LiCoO2. 4.0 V was initially utilized to isolate the Zn-Li alloying, which we expected to complete at 4.2 V, from the conversion reaction. However, the results at both potentials were reasonably

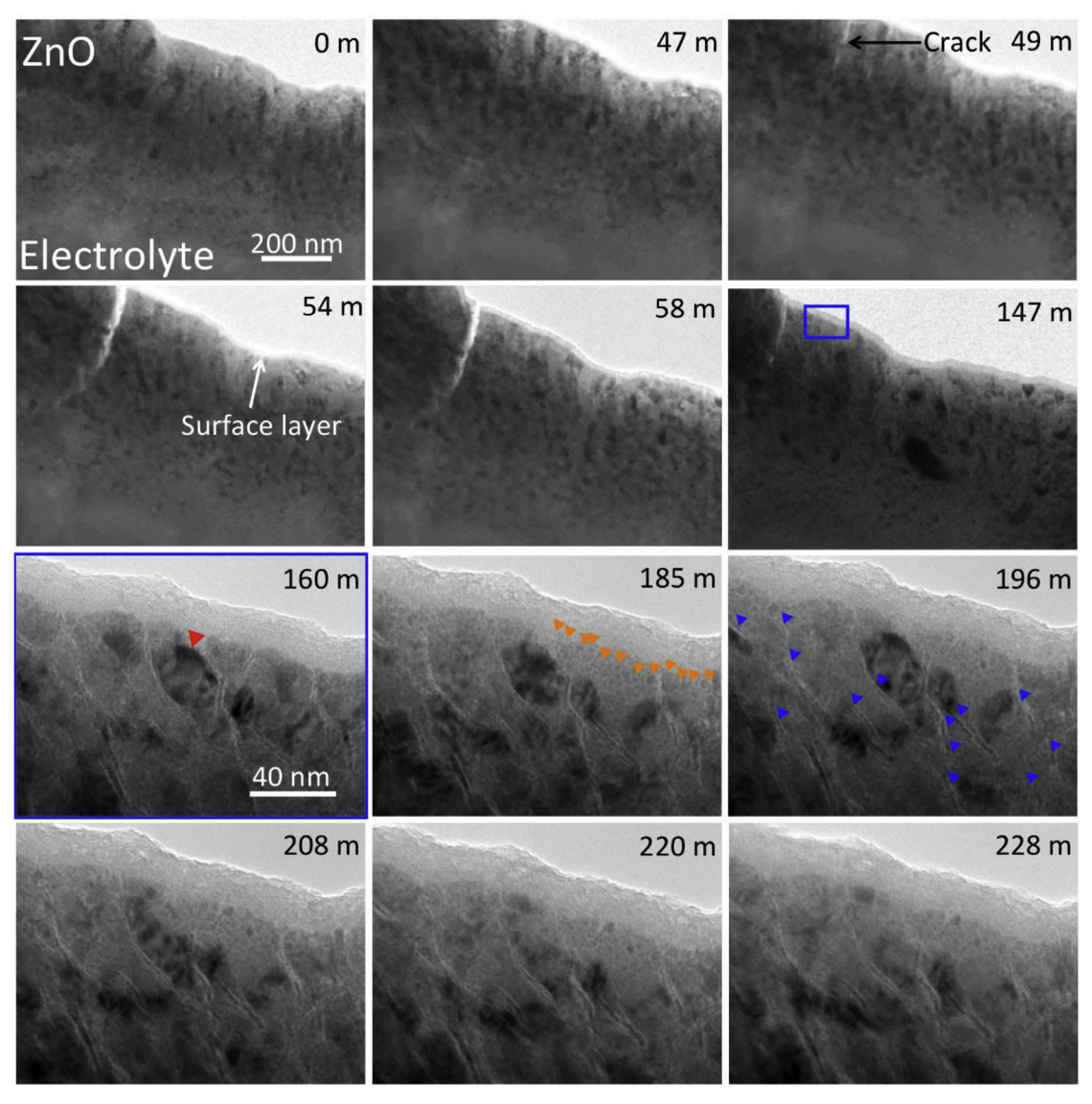


Fig. 4. *Operando* TEM during ZnO lithiation at 4.2 V. The blue square in the lower magnification images highlights the region observed at higher magnification. The triangles in the images highlight (red) a ZnO grain that subsequently reacts and loses its diffraction contrast, (orange) small metal nanoparticle precipitates formed from the conversion reaction, and (blue) product phase that initially forms preferentially along the grain boundaries. (For interpretation of the references to colour in this figure legend, the reader is referred to the Web version of this article.)

consistent. Since the in situ XPS suggests Zn becomes more oxidized, rather than reduced, lithiation of the sample was continued ex situ in an Ar filled glovebox for 10 h in order to check the results. Cycling ex situ causes the Auger peak to shift back to that associated with ZnO. A similar trend is observed for the Zn 2p_{3/2}, which shifts to higher binding energies when cycled in situ and back toward the pristine value when cycled ex situ. Comparing the Zn 2p3/2 and Zn Auger peak energies to Wagner chemical state plots [33] suggests that Zn occurs as ZnO when cycled ex situ. When lithiated in situ it is primarily ZnCO₃. This agrees well with the large $\mathrm{CO_2}^{3-}$ related peaks at 531.3 eV in the O 1s and 288.0 eV in the C 1s observed from the sample reacted in situ. The pristine and ex situ cycled samples primarily have oxide and hydroxide peaks in the O 1s. After charging in situ the sample in the chamber was dark, comparable to the material observed in the optical microscope, however the Li 1s peak was relatively small and noisy. This weak Li signal also motivated us to continue the reaction ex situ for 10 h to ensure complete lithiation. However, after this additional 10 h, the Li 1s peak was still similarly small and noisy, indicating that lithium oxide is depleted from the surface relative to the bulk. We hypothesize that in vacuum reduced Zn at the surface, will rapidly form carbonate

 $(\Delta H_{ZnCO_3}^f \approx -817 \text{ kJ mol}^{-1})$ [34] which dominates the near surface chemistry; i.e. to the depth resolution of XPS. In oxygen-rich environments the reaction favours ZnO formation. Surface carbonate tends to dominate on many electrodes cycled in ultrahigh vacuum and organic liquid electrolyte due to the presence of some CO/CO₂ and organics. Surface carbonate has important implications in affecting cycle life and has been shown to be sensitive to electrode chemistry [32]. This reaction may, in part, explain the relatively thick surficial amorphous layer on reacted ZnO as compared to several other reported conversion electrode chemistries with lower carbonate formation enthalpies [2]. It will never be possible to utilize XPS to observe the solid-liquid interface in situ, since it is by definition a buried interface. However, opportunities exist to apply this type of cell in existing differentially pumped high-pressure XPS systems and observe surface reactions in model gaseous environments at controlled chemical potentials in order to gain insights into fundamental surface reactions.

Fig. 4 shows time-lapse *operando* TEM images of an initially 250 nm ZnO film that was thinned to < 100 nm in the region of observation using FIB milling. Initial imaging occurred at lower magnification to observe the overall response of the sample. Bend contour motion,

indicating strain, is observed in the early stages of reaction and at ≈49 min a crack develops at the surface (see Video S3). Internal cracking could explain the profilometry result suggesting a larger volume expansion than predicted theoretically. At approximately the same time, an amorphous surface film begins to form and grows to \approx 20 nm. This is assumed to correspond with the film formation step observed in AFM and to have ZnCO3 surface chemistry as suggested by XPS performed in vacuum. The surface crack subsequently partially closes, due to continued expansion of the surrounding regions. Higher magnification images were acquired after 147 min. At this magnification, it can be seen that the reaction initially penetrated the grain boundaries, with certain boundaries being kinetically favoured, likely due to boundary anisotropy. The conversion reaction is observed through the progressive loss of diffraction contrast in the grains and the appearance and growth of small second phase Zn-Li particles (see orange triangles in Fig. 4 for examples). The red triangle in Fig. 4 highlights a grain with clearly observable diffraction contrast. By 228 min, this contrast is almost completely eliminated due to the conversion reaction. The progression of this reaction may also be seen in Video S4. The lack of metallic nanoparticle percolation is observed in the TEM, which agrees with the relatively high electrical resistance of the lithiated material. In situ Li-ZnO reactions have been reported for both nanoparticles and nanowires at -3 V and -4 V versus Li metal, respectively [35,36]. Our results exhibit similar features as those reported previously, such as the formation of a thick surficial film, cracking during lithiation, and the formation of metallic nanoparticles. The goal of this TEM work was to demonstrate analogous results in a cell cycled within a voltage window relevant to Li ion batteries and correlate with our other operando and in situ results obtained from the same electrochemical cell.

This work demonstrated a convenient pseudo-solid-state electrochemical cell that is configurable for a variety of *in situ* and *operando* characterization methodologies, including; optical imaging, AFM, XPS, TEM, and XRD. The methodology circumvents prior challenges associated with X-ray beam interactions with ionic liquid electrolyte during *in situ* XPS and control of potential during most open-cell *in situ* TEM experiments, and creates a host of opportunities for performing multiplatform comparative studies of Li ion reactions under electrochemically well controlled conditions. Here we utilized a combination of XPS, AFM, and TEM to gain new insights into both the structure and chemistry of amorphous carbonate-rich surface layers forming on ZnO. While a combination of electrical measurements, optical imaging, XRD, and TEM provided insights into the reaction pathways associated with the ZnO conversion and Zn alloying reactions over multiple length scales and their correlations with electrical properties.

Acknowledgements

We acknowledge support from United States National Science Foundation under Grant No. 1254406. This work was carried out in part at the Materials Research Laboratory Central Research Facilities, University of Illinois. We would also like to acknowledge Dr. M. Sardela, R.T. Haasch, K. Walsh, and W. Swiech for their assistance with testing customized XRD, XPS, AFM, and TEM stages.

Appendix A. Supplementary data

Supplementary data related to this article can be found at https://doi.org/10.1016/j.jpowsour.2018.08.029.

References

- R.R. Chianelli, J.C. Scanlon, B.M.L. Rao, J. Electrochem. Soc. 125 (1978) 1563–1566.
- [2] X.H. Liu, J.Y. Huang, Energy Environ. Sci. 4 (2011) 3844-3860.
- [3] A.M. Tripathi, W.-N. Su, B.J. Hwang, Chem. Soc. Rev. 47 (2018) 736–851.
- [4] W.-S. Yoon, C.P. Grey, M. Balasubramanian, X.-Q. Yang, J. McBreen, Chem. Mater. 15 (2003) 3161–3169.
- [5] P. Novák, J.C. Panitz, F. Joho, M. Lanz, R. Imhof, M. Coluccia, J. Power Sources 90 (2000) 52–58.
- [6] J.N. Reimers, J.R. Dahn, J. Electrochem. Soc. 139 (1992) 2091-2097.
- [7] M. Roberts, J.J. Biendicho, S. Hull, P. Beran, T. Gustafsson, G. Svensson, K. Edström, J. Power Sources 226 (2013) 249–255.
- [8] P.P.R.M.L. Harks, F.M. Mulder, P.H.L. Notten, J. Power Sources 288 (2015) 92–105.
- [9] Z.-H. Xie, Z. Jiang, X. Zhang, J. Electrochem. Soc. 164 (2017) A2110–A2123.
- [10] J. Lu, T. Wu, K. Amine, Nature Energy 2 (2017) 17011.
- [11] K.W. Noh, S.J. Dillon, Scripta Mater. 69 (2013) 658-661.
- [12] C.-M. Wang, X. Li, Z. Wang, W. Xu, J. Liu, F. Gao, L. Kovarik, J.-G. Zhang, J. Howe, D.J. Burton, Z. Liu, X. Xiao, S. Thevuthasan, D.R. Baer, Nano Lett. 12 (2012) 1624–1632.
- [13] X.H. Liu, Y. Liu, A. Kushima, S. Zhang, T. Zhu, J. Li, J.Y. Huang, Advanced Energy Materials 2 (2012) 722–741.
- [14] R.R. Unocic, L. Baggetto, G.M. Veith, J.A. Aguiar, K.A. Unocic, R.L. Sacci, N.J. Dudney, K.L. More, Chem. Commun. 51 (2015) 16377–16380.
- [15] R.L. Sacci, N.J. Dudney, K.L. More, L.R. Parent, I. Arslan, N.D. Browning, R.R. Unocic, Chem. Commun. 50 (2014) 2104–2107.
- [16] C.M. Wang, W. Xu, J. Liu, D.W. Choi, B. Arey, L.V. Saraf, J.G. Zhang, Z.G. Yang, S. Thevuthasan, D.R. Baer, N. Salmon, J. Mater. Res. 25 (2011) 1541–1547.
- [17] Z. Wang, D. Santhanagopalan, W. Zhang, F. Wang, H.L. Xin, K. He, J. Li, N. Dudney, Y.S. Meng, Nano Lett. 16 (2016) 3760–3767.
- [18] C.-Y. Tang, R.T. Haasch, S.J. Dillon, Chem. Commun. 52 (2016) 13257-13260.
- [19] C.-Y. Tang, K. Leung, R.T. Haasch, S.J. Dillon, ACS Appl. Mater. Interfaces 9 (2017) 33968–33978.
- [20] K. Kerman, A. Luntz, V. Viswanathan, Y.-M. Chiang, Z. Chen, J. Electrochem. Soc. 164 (2017) A1731–A1744.
- [21] J. Christensen, P. Albertus, R.S. Sanchez-Carrera, T. Lohmann, B. Kozinsky, R. Liedtke, J. Ahmed, A. Kojic, J. Electrochem. Soc. 159 (2011) R1–R30.
- [22] C. Yu, S. Ganapathy, E.R.H.v. Eck, H. Wang, S. Basak, Z. Li, M. Wagemaker, Nat. Commun. 8 (2017) 1086.
- [23] A.C. Luntz, J. Voss, K. Reuter, J. Phys. Chem. Lett. 6 (2015) 4599-4604.
- [24] J.H. Woo, J.E. Trevey, A.S. Cavanagh, Y.S. Choi, S.C. Kim, S.M. George, K.H. Oh, S.-H. Lee, J. Electrochem. Soc. 159 (2012) A1120–A1124.
- [25] J. Wang, P. King, R.A. Huggins, Solid State Ionics 20 (1986) 185–189.
- [26] H. Usui, T. Kono, H. Sakaguchi, Novel Composite Thick-film Electrodes Consisted of Zinc Oxide and Silicon for Lithium-ion Battery Anode, (2012).
- [27] F. Wu, G. Yushin, Energy Environ. Sci. 10 (2017) 435-459.
- [28] Shilpa, B.M. Basavaraja, S.B. Majumder, A. Sharma, J. Mater. Chem. 3 (2015) 5344–5351.
- [29] H. Wang, Q. Pan, Y. Cheng, J. Zhao, G. Yin, Electrochim. Acta 54 (2009) 2851–2855.
- [30] Y. Hwa, J.H. Sung, B. Wang, C.-M. Park, H.-J. Sohn, J. Mater. Chem. 22 (2012) 12767–12773.
- [31] C.-Y. Tang, L. Feng, R.T. Haasch, S.J. Dillon, Electrochim. Acta 277 (2018)
- [32] C.-Y. Tang, Y. Ma, R.T. Haasch, J.-H. Ouyang, S.J. Dillon, J. Phys. Chem. Lett. 8 (2017) 6226–6230.
- [33] C.D. Wagner, G.E. Muilenberg, Handbook of X-ray Photoelectron Spectroscopy: a Reference Book of Standard Data for Use in X-ray Photoelectron Spectroscopy, Perkin-Elmer, 1979.
- [34] H.T. Haselton, J.R. Goldsmith, Geochem. Cosmochim. Acta 51 (1987) 261–265.
- [35] S. Qingmei, D. Zimin, Z. Jun, D. Gaohui, X. Bingshe, Nanotechnology 24 (2013) 255705.
- [36] A. Kushima, X.H. Liu, G. Zhu, Z.L. Wang, J.Y. Huang, J. Li, Nano Lett. 11 (2011) 4535–4541.